



Performance analysis of enhanced radiative cooling of solar cells based on a commercial silicon photovoltaic module

Bin Zhao, Mingke Hu, Xianze Ao, Gang Pei*

Department of Thermal Science and Energy Engineering, University of Science and Technology of China, Hefei 230027, China

ARTICLE INFO

Keywords:

Radiative cooling
Solar cell
Glass cover
Photovoltaic module

ABSTRACT

Recent research on cooling solar cells through the radiative cooling method has elicited much interest. Compared with bare silicon solar cells, modified cells with enhanced radiative cooling can reduce temperature by over 10 °C, thereby improving the photovoltaic conversion efficiency of solar cells. At present, the commercial silicon photovoltaic (PV) module is the mainstream product for PV application. Thus, investigating the effect of enhanced radiative cooling on cooling solar cells based on a commercial PV module is imperative. In this study, the effect of enhanced radiative cooling on solar cells based on a commercial PV module was explored, and the application prospect was analyzed preliminarily. A sample of PV module (referred to as “commercial structure” hereinafter) was fabricated by encapsulating a bare crystalline silicon cell with glass. The spectral property of the commercial structure was modified by adding a polydimethylsiloxane (PDMS) film on its top surface; this structure is referred to as “modified structure” hereinafter. A comparative experiment was conducted, and results showed that the solar cell temperatures in the commercial and modified structures were almost consistent. The effects of enhanced radiative cooling on the PV module under different conditions were also analyzed theoretically through a universal mathematical model. Simulation results revealed that the solar cell temperature could only be reduced by 1.75 K even in the ideal case. Experimental and simulation results indicated that enhanced radiative cooling based on a PV module shows no specific potential for cooling solar cells in actual settings. The performance of enhanced radiative cooling for solar cells in an extraterrestrial environment was also discussed preliminarily, and the results showed that radiative cooling can be applied as an alternative method for the thermal management of solar cells in the extraterrestrial environment.

1. Introduction

Single-gap silicon solar cells possess limited photovoltaic (PV) efficiency (Martí and Araújo, 1996; Shockley and Queisser, 1961). Thus, only a part of solar irradiation is converted into electricity, and the remaining absorbed solar irradiation dissipates as heat and thus increases the operating temperature of solar cells. However, the high operating temperatures of solar cells weaken the cells' PV performance. For example, for every 1 K increase in temperature, the relative efficiency of crystalline silicon solar cells decreases by approximately 0.45% (Skoplaki and Palyvos, 2009). Therefore, decreasing the operating temperature of solar cells is necessary.

Recent investigations on solar cell radiative cooling has elicited much interest (Safi and Munday, 2015; Zhou et al., 2016; Zhu et al., 2015, 2014). Radiative cooling (Bagiorgas and Mihalakakou, 2008; Chen et al., 2016; Cui et al., 2016; Dyreson and Miller, 2016; Gentle et al., 2013; Hu et al., 2016; Lu et al., 2016; Man et al., 2011; Raman

et al., 2014; Rephaeli et al., 2013; Zeyghami et al., 2018; Zhai et al., 2017) is a passive cooling technique that does not use any extra power input. The atmosphere exhibits high transmittance for electromagnetic waves between 8 and 13 μm (atmospheric window), coinciding with the peak thermal radiation of objects at a typical ambient temperature. Thus, objects exposed to the sky can obtain cooling energy and/or be cooled passively by radiating heat to outer space, where the temperature is close to absolute zero. Under this circumstance, the key to cooling solar cells via the passive radiative cooling method is to improve the mid-infrared (i.e., > 4 μm) thermal emissivity of solar cells. Thus, various solutions have been proposed to optimize the mid-infrared thermal properties of solar cells. This study focused on silicon solar cells because they are still the mainstream product on the market. Zhu et al. (Zhu et al., 2015, 2014) used the photonic approach to design and fabricate several photonic structures, which act as additional radiative coolers on the top of solar cells to improve the mid-infrared thermal emissivity of cells. Zhu et al. designed a silica planar cooler

* Corresponding author.

E-mail address: peigang@ustc.edu.cn (G. Pei).

<https://doi.org/10.1016/j.solener.2018.10.043>

Received 3 May 2018; Received in revised form 13 August 2018; Accepted 11 October 2018

Available online 17 October 2018

0038-092X/ © 2018 Elsevier Ltd. All rights reserved.

Nomenclature		c_0	velocity of light, $\text{m}\cdot\text{s}^{-1}$
T_{top}	temperature of the top surface, K	\dot{q}	internal heating source, $\text{W}\cdot\text{m}^{-2}$
T_{bottom}	temperature of the bottom surface, K	<i>Greek symbols</i>	
T_{amb}	ambient temperature, K	α	absorptivity of the structure
T_{ground}	ground temperature, K	ε	emissivity of the structure
P_{rad}	power radiated by the top surface, $\text{W}\cdot\text{m}^{-2}$	ε_{sky}	emissivity of the atmosphere
P_{sky}	absorbed power from the atmosphere, $\text{W}\cdot\text{m}^{-2}$	λ	wavelength, μm
$P_{non-rad}$	power due to conductive and convective processes, $\text{W}\cdot\text{m}^{-2}$	θ	radiation angle, rad
P_{sun}	absorbed power from the sun, $\text{W}\cdot\text{m}^{-2}$	<i>Abbreviations</i>	
$J_{\lambda,b}$	spectral radiance of a blackbody, $\text{W}\cdot\text{m}^{-2}\cdot\text{sr}^{-1}\cdot\mu\text{m}^{-1}$	EVA	Ethylene-Vinyl-Acetate
h	Planck constant	TPT	Tedlar-Polyester-Tedlar
k_B	Boltzmann constant	PDMS	polydimethylsiloxane
k	thermal conductivity, $\text{W}\cdot\text{m}^{-1}\cdot\text{K}^{-1}$	PV	photovoltaic
h_{top}	heat transfer coefficient at the top surface, $\text{W}\cdot\text{m}^{-2}\cdot\text{K}^{-1}$		
h_{bottom}	heat transfer coefficient at the bottom surface, $\text{W}\cdot\text{m}^{-2}\cdot\text{K}^{-1}$		
G	solar radiation, $\text{W}\cdot\text{m}^{-2}$		

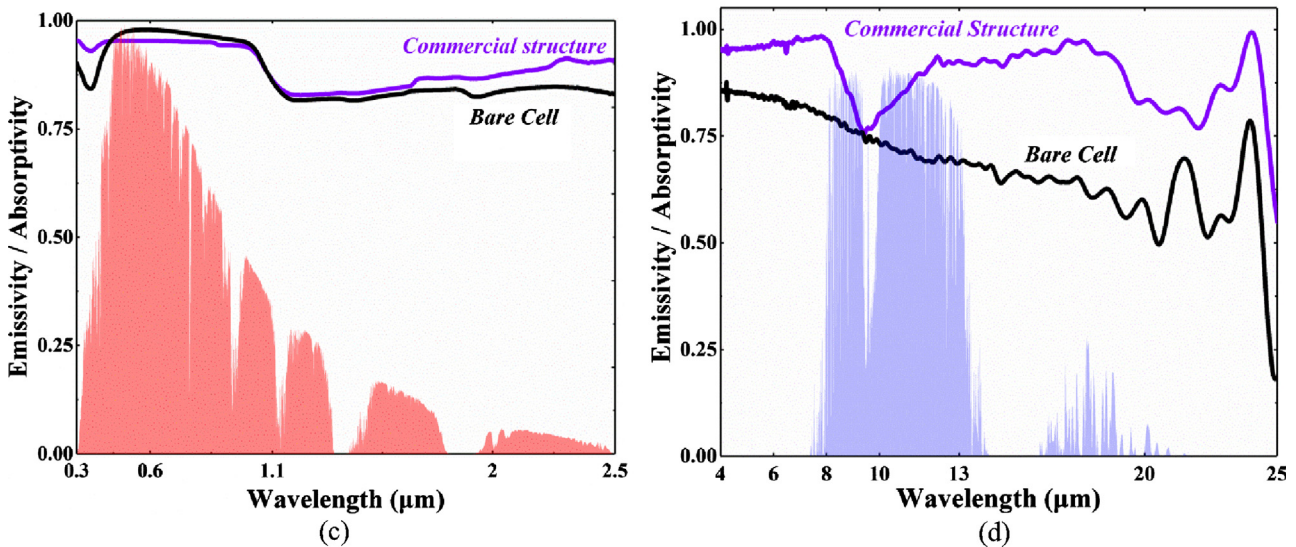
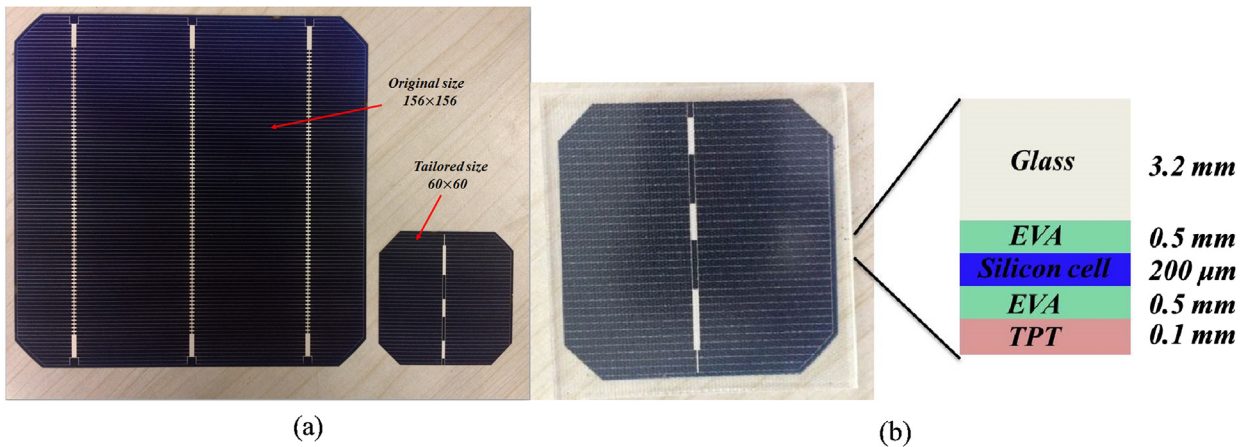


Fig. 1. (a) Commercial crystalline silicon solar cell. The cell possesses a screen-printed silver front and aluminum rear contacts. (b) Encapsulated silicon solar cell (commercial structure) with a cross-section schematic. The encapsulated structure includes a 3.2 mm glass cover, two EVA (Ethylene-Vinyl-Acetate) layers, a silicon cell, and a TPT (Tedlar-Polyester-Tedlar) layer. (c) Measured emissivity/absorptivity of the bare cell (black curve) and commercial structure (violet curve) over the main solar radiation band, with the normalized AM 1.5 solar spectrum plotted as a reference (red). (d) Measured emissivity/absorptivity of the bare cell (black curve) and commercial structure (violet curve) over the mid-infrared band, with an atmospheric spectral transmittance profile (blue) as a reference. (For interpretation of the references to colour in this figure legend, the reader is referred to the web version of this article.)

with a 2D square lattice of pyramids on the top (Zhu et al., 2014) and placed this cooler on the top of a solar cell for self-cooling. Simulation showed that the temperature of the silicon solar cell decreased by 17.6 K after adding the silica pyramid-based cooler on the top of the solar cell; this temperature decrement significantly improved photovoltaic conversion efficiency. Afterward, the same group (Zhu et al., 2015) proposed another photonic crystal structure as an enhanced radiative cooler. This cooler was experimentally fabricated by etching a square lattice of air hole-based microstructure into a double-side-polished fused silica wafer. The outdoor experiment was performed under direct sunlight, and the results showed that the temperature of a silicon solar cell with this radiative cooler can be reduced by as much as 13 °C, indicating that the radiative cooling method has a potential for cooling solar cells passively. However, these studies used laboratory-simulated silicon solar cells rather than commercial-actual ones. The spectral properties of the simulated cells were simplified, and the cells had relatively low emissivity in the mid-infrared wavelength band, unlike commercial silicon cells. Thus, the experimental and simulation results obtained deviate strongly from actual values. In addition, if the radiative cooling method is used for cooling silicon solar cells in actual

applications, the effect of the glass cover integrated into the PV module should be considered. Therefore, investigating the effect of enhanced radiative cooling of cooling solar cells based on PV modules, rather than simulating solar cells, is necessary in real applications. The potential and feasibility of using radiative cooling technology to passively cool solar cells for common PV modules are analyzed in this investigation on the basis of engineering practice rather than pure theoretical exploration.

In this study, the effects of enhanced radiative cooling on solar cells based on a PV module were investigated for practical applications. A crystalline silicon solar cell was encapsulated with 3.2 mm glass in accordance with the crafting procedure of a commercial PV module (referred to as “commercial structure” hereafter). Then, the mid-infrared spectral emissivity of the commercial structure was improved to enhance its radiative cooling by coating the glass with a polydimethylsiloxane (PDMS) film (referred to as “modified structure” hereafter). A comparative experiment was conducted, and nearly similar solar cell temperatures were observed between the commercial and modified structures. Moreover, the effects of enhanced radiative cooling on solar cells based on a PV module under different conditions

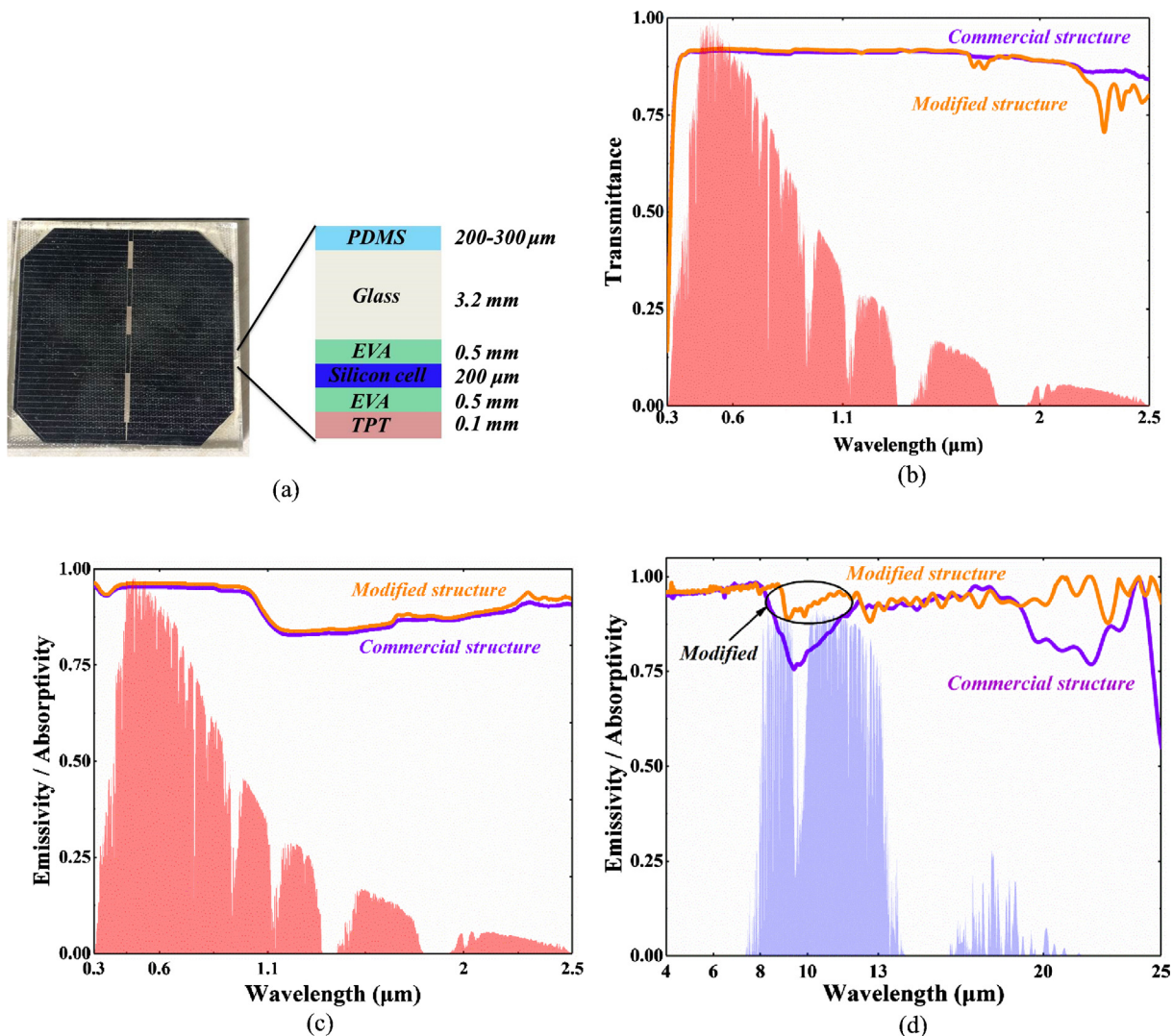


Fig. 2. (a) Modified structure with a cross-section schematic. The commercial structure was modified by coating a PDMS film on the top of a 3.2 mm glass. (b) Measured transmittance of glass with a PDMS film (orange curve) and without a PDMS film (violet curve) over the main solar radiation band, with the normalized AM 1.5 solar spectrum plotted as a reference (red). (c) Measured emissivity/absorptivity of the modified structure (orange curve) and commercial structure (violet curve) over the main solar radiation band, with the normalized AM 1.5 solar spectrum plotted as a reference. (d) Measured emissivity/absorptivity of the modified structure (orange curve) and commercial structure (violet curve) over the mid-infrared band, with an atmospheric spectral transmittance profile (blue) as a reference. (For interpretation of the references to colour in this figure legend, the reader is referred to the web version of this article.)

(e.g., sky condition and solar irradiance) were analyzed theoretically through a universal mathematical model for PV modules with different optimized spectral properties. Then, the performance of enhanced radiative cooling for solar cells in an extraterrestrial environment was preliminarily discussed.

2. Description of the experimental setup

2.1. Spectral characterization

A typical commercial crystalline silicon solar cell (Fig. 1a) (referred to as “bare cell” hereafter) with screen-printed silver front and aluminum rear contacts was selected in this study. The bare cell was encapsulated with 3.2 mm glass (commercial structure) to authentically illustrate the effects of enhanced radiative cooling for solar cells in practice. The encapsulated structure (Fig. 1b) was similar to the commercial PV module. The spectral emissivity/absorptivity of the bare cell and commercial structure was measured with a UV–Vis–NIR spectrophotometer (DUV-3700) and Fourier transform infrared spectrophotometer (Nicolet iS10). The results are shown in Fig. 1c and d.

The bare cell and commercial structure showed good solar absorption in the solar radiation band (Fig. 1c). The band gap of the crystalline silicon solar cell was approximately 1.1 eV, which corresponds to a 1.1 μm wavelength. Thus, the bare cell and commercial structure exhibited strong light absorption in the wavelength range of 0.3–1.1 μm , where the light energy was above the band gap of the silicon solar cell and can be converted to electricity. However, in the wavelength range of 1.1–2.5 μm , the bare cell and commercial structure also presented high absorptivity most likely due to the heavily doped regions and the presence of metal contacts in the cells (Li et al., 2017). Therefore, the extra absorbed solar radiation that cannot be converted to electricity is dissipated to heat and increases the operating temperature of the solar cells.

Fig. 1d implies that the commercial structure showed greater emissivity than the bare cell in the majority of the wavelength range of 4–25 μm . This finding can be explained by the 70%–80% silica content of 3.2 mm glass in the commercial structure (Kurkjian and Prindle, 2005). Silica is a low-index material and optically transparent to solar radiation. It exhibits a relatively high extinction coefficient over the thermal radiation band at a typical temperature. This property is fit for thermal radiation enhancement. However, silica has a negative permittivity near 9 μm because of its strong phonon–polariton resonance. This negative permittivity leads to a large reflectivity and a corresponding small emissivity. This information can explain the emissivity decline at approximately 9 μm in Fig. 1d. Such a decline in emissivity weakens the effect of radiative cooling on solar cells. To improve the mid-infrared emissivity of the commercial structure and enhance the potential of its radiative cooling, we placed a polydimethylsiloxane (PDMS) film on the top of the glass (Fig. 2a). The PDMS film was coated by hand, followed by curing for 6 h at 60 $^{\circ}\text{C}$. The product was the modified structure. The spectral transmittance of the glass with the PDMS film in the wavelength range of 0.3–2.5 μm (Fig. 2b) was tested

to ensure that the additional PDMS film does not damage the optical transparency of the glass and thus guarantees the optical efficiency of the module. The spectral emissivity values in the wavelength ranges of 0.3–2.5 μm and 4–25 μm were also measured and are shown in Fig. 2c and d. Compared with recent studies that used photonic approaches (Zhou et al., 2016; Zhu et al., 2015, 2014), this study selected a PDMS film to enhance radiative cooling. This strategy is cheaper and more convenient than other methods. Notably, all of these methods, including photonic approaches and PDMS film use, aim to enhance the mid-infrared emissivity of solar cells for cooling, and the modified spectral properties are similar.

2.2. Experimental setup

The experimental structures included commercial and modified structures, which are shown in Fig. 1b and 2a, respectively. A schematic of the test setup is presented in Fig. 3a, and an actual photo of the test setup is provided in Fig. 3b. The two structures (commercial and modified) were fixed in the aperture side by side with a transparent packaging tape for support. Thermocouples (T Type) were attached to the backside of the structure to monitor the temperature of the silicon cells, and a pyranometer (TBQ-2A) was utilized to measure the total solar radiation. All data were recorded by a data acquisition instrument (Agilent 34970A). A list of experimental measurement and monitoring devices and their uncertainties is provided in Table 1. The experimental setup was exposed to the sky directly on a building roof in Hefei, a city in eastern China (32 $^{\circ}$ N, 117 $^{\circ}$ E), and the test setup was tilted 30 $^{\circ}$ toward the south to maximize the solar radiation received by the test structures.

3. Thermal analysis

A quasi-steady-state mathematical model was developed to evaluate the effects of enhanced radiative cooling for solar cells under different conditions. A schematic of the model is shown in Fig. 4. The presented structure consisted of a commercial structure and a specific surface (without thickness). We assumed that such a specific surface can optimize the spectral property of the commercial structure on the basis of spectral control technologies in the present or future.

The temperature variation of the structure in the horizontal direction was ignored because it was small. Moreover, the total absorbed solar radiation by the structure was assumed to be contributed only by the solar cell and entirely converted to heat. Thus, the steady-state heat diffusion equation is expressed as follows (Bergman et al., 2011; Li et al., 2017; Zhu et al., 2014):

$$\frac{d}{dz} \left(k \frac{dT}{dz} \right) + \dot{q} = 0, \quad (1)$$

where T is the temperature distribution along the z direction (K) and k is the thermal conductivity of the structure along the z direction ($\text{W}\cdot\text{m}^{-1}\cdot\text{K}^{-1}$). In particular, the thermal conductivities of glass, EVA, silicon solar cell, and TPT were 0.98, 0.24, 1.48, and 0.36 $\text{W}\cdot\text{m}^{-1}\cdot\text{K}^{-1}$,

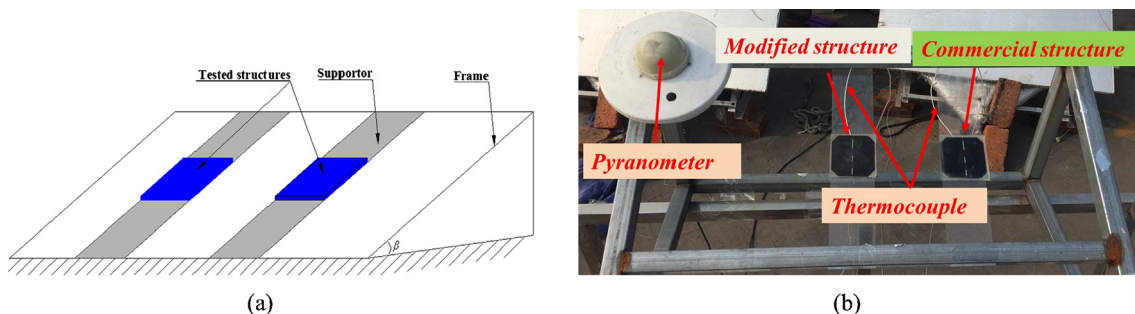


Fig. 3. (a) Schematic of the test setup. (b) Actual setup with a pyranometer on a rooftop in Hefei, China.

Table 1
List of experimental measurement and monitoring devices.

Name of devices	Specification	Uncertainty
Pyranometer	TBQ-2A	± 2%
Thermocouple	Type T (copper-constantan)	± 0.5 °C
Data acquisition instrument	Agilent 34970A	/

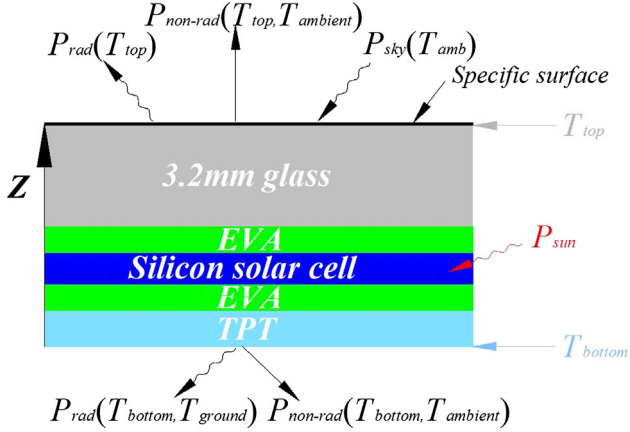


Fig. 4. Schematic of the 1D thermal mathematical model. The presented structure consisted of a commercial structure and a specific surface (without thickness). Such a specific surface was assumed to optimize the spectral property of the commercial structure. T_{top} and T_{bottom} refer to temperature at the top and bottom surfaces, respectively. T_{amb} is the ambient temperature. T_{ground} is the temperature of the ground. $P_{non-rad}$ is the comprehensive effect of convection and conduction.

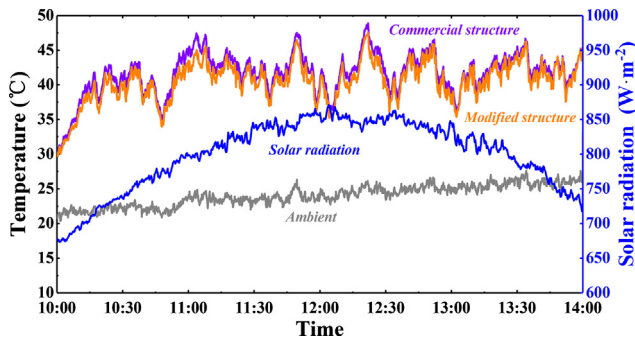


Fig. 5. Temperature of solar cells in the commercial structure (violet curve) and modified structure (orange curve). Ambient temperature (gray curve) and solar radiation (blue curve) are also plotted as a reference. (For interpretation of the references to colour in this figure legend, the reader is referred to the web version of this article.)

respectively (Lee et al., 2008). \dot{q} is the internal heating source provided by the absorbed solar radiation.

The boundary conditions of such a model are as follows:

At the top surface:

$$-k \frac{dT}{dz} \Big|_{z=z_{max}} = P_{rad}(T_{top}) - P_{sky}(T_{amb}) + P_{non-rad}(T_{top}, T_{amb}), \quad (2)$$

Table 2
Tested T_{bottom} and simulated T_{bottom} in the modified structure.

Time Point	11:00	11:10	11:20	11:30	11:40	11:50	12:00	12:10	12:20	12:30	12:40	12:50	13:00
Tested T_{bottom} (°C)	41.8	41.7	42.7	41.2	41.2	45.8	39.5	42.3	46.0	39.6	43.0	43.6	38.6
Simulated T_{bottom} (°C)	42.0	42.4	43.6	43.4	40.4	44.5	42.5	41.0	43.9	41.5	40.1	44.4	40.0
RMSD (%)	4.14%												

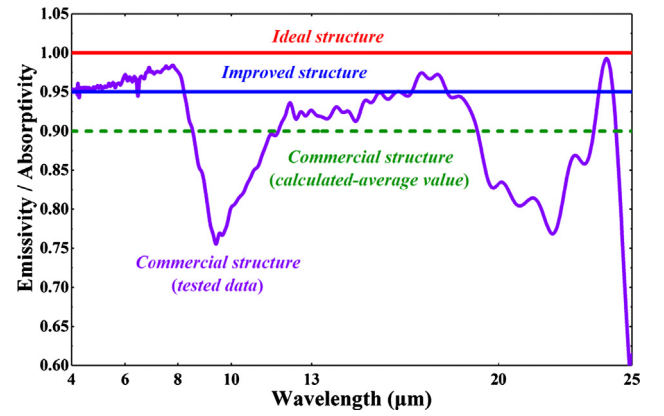


Fig. 6. Emissivity/absorptivity of the commercial structure (violet curve), improved structure (blue curve), and ideal structure (red curve). The dashed curve (green curve) is the average emissivity of the commercial structure. (For interpretation of the references to colour in this figure legend, the reader is referred to the web version of this article.)

At the bottom surface:

$$k \frac{dT}{dz} \Big|_{z=0} = P_{non-rad}(T_{bottom}, T_{amb}) + P_{rad}(T_{bottom}, T_{ground}). \quad (3)$$

In Eq. (1), the internal heating source \dot{q} is determined by

$$\dot{q} = G \cdot \alpha, \quad (4)$$

where G is the total solar radiation, $\text{W}\cdot\text{m}^{-2}$. α is the solar absorptivity of the structure, weighted by the standard AM 1.5 solar spectrum.

In Eq. (2), $P_{rad}(T_{top})$ is the power density radiated by the top surface.

$$P_{rad}(T_{top}) = \int_0^\infty \int_0^{2\pi} \int_0^{\pi/2} I_{\lambda,b}(\lambda, T_{top}) \varepsilon(\lambda, \theta, \varphi) \cos\theta \sin\theta d\theta d\varphi d\lambda, \quad (5)$$

where $\varepsilon(\lambda, \theta, \varphi)$ denotes the directional spectral emissivity of the structure that is obtained from the measured data, as shown in Fig. 2(c) and (d). $I_{\lambda,b}(\lambda, T_{top})$ is the spectral radiance of a blackbody at temperature T_{top} , and can be expressed as follows (Bergman et al., 2011):

$$I_{\lambda,b}(\lambda, T_{top}) = \frac{2hc_0^2}{\lambda^5 \{ \exp [hc_0/(\lambda k_B T_{top})] - 1 \}}, \quad (6)$$

where h is the Planck constant ($h = 6.626 \times 10^{-34}$ J·s), k_B is the Boltzmann constant ($k_B = 1.381 \times 10^{-23}$ J·K⁻¹), and c_0 is the velocity of light ($\text{m}\cdot\text{s}^{-1}$).

$P_{sky}(T_{amb})$ is the absorbed power density from the atmosphere, which is calculated by

$$P_{sky}(T_{amb}) = \int_0^\infty \int_0^{2\pi} \int_0^{\pi/2} I_{\lambda,b}(\lambda, T_{amb}) \alpha(\lambda, \theta, \varphi) \varepsilon_{sky}(\lambda, \theta, \varphi) \cos\theta \sin\theta d\theta d\varphi d\lambda, \quad (7)$$

where $\alpha(\lambda, \theta, \varphi)$ is the spectral and angular absorptivity of the structure, which is equal to $\varepsilon(\lambda, \theta, \varphi)$ according to Kirchhoff's radiation law. $\varepsilon_{sky}(\lambda, \theta, \varphi)$ is the spectral and angular emissivity of the atmosphere, which can be derived from a single correlation by using the precipitable water vapor amount as the only input parameter (Das and Iqbal, 1987).

In Eqs. (2) and (3), $P_{non-rad}(T, T_{amb})$ is the power density caused by

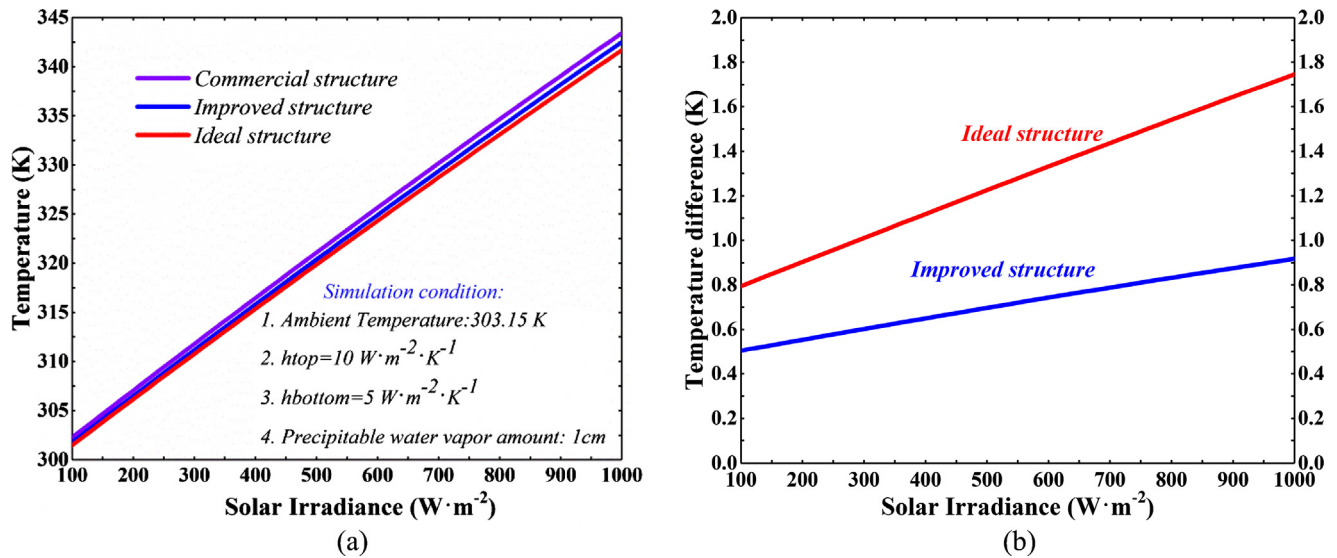


Fig. 7. (a) Temperature of solar cells in the commercial structure (violet curve), improved structure (blue curve), and ideal structure (red curve) under different solar irradiances. h_{top} and h_{bottom} were set to 10 and $5 W \cdot m^{-2} \cdot K^{-1}$, respectively. Ambient temperature and precipitable water vapor amount were 303.15 K and 1 cm, respectively. (b) Temperature difference between the solar cell of the commercial structure and that of the improved structure (blue curve) and ideal structure (red curve) under different solar irradiances. (For interpretation of the references to colour in this figure legend, the reader is referred to the web version of this article.)

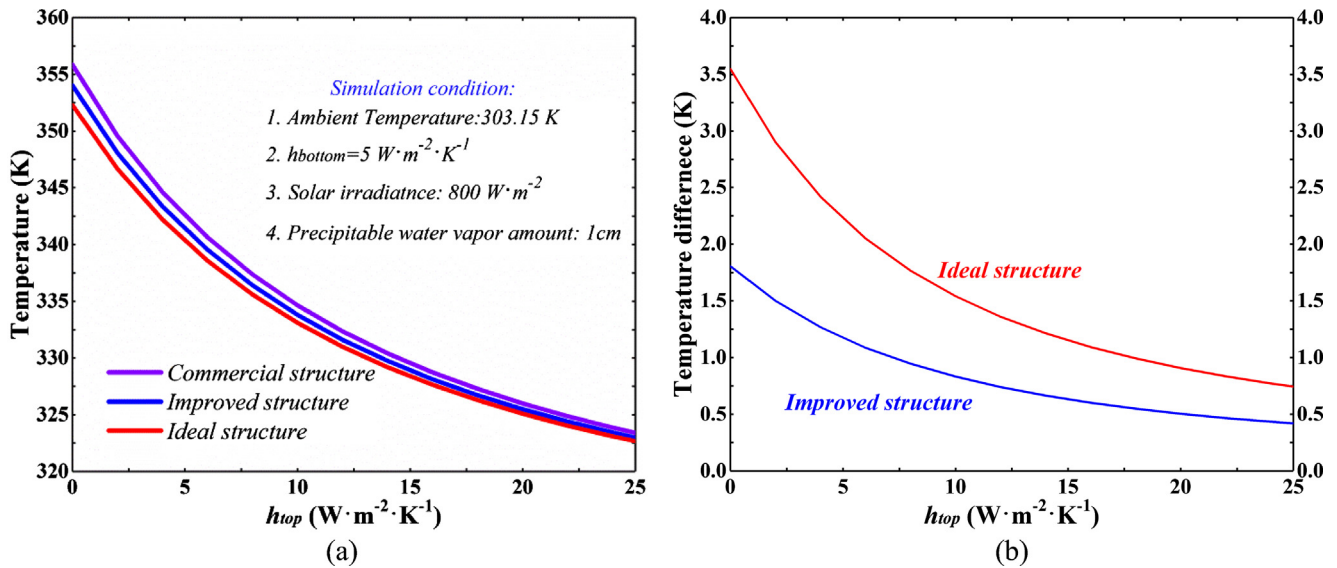


Fig. 8. (a) Temperature of solar cells in the commercial structure (violet curve), improved structure (blue curve), and ideal structure (red curve) under different h_{top} values. h_{bottom} was set to $5 W \cdot m^{-2} \cdot K^{-1}$. Ambient temperature, solar radiation, and precipitable water vapor amount were set to 303.15 K, $800 W \cdot m^{-2}$, and 1 cm, respectively. (b) Temperature difference of solar cells between the commercial and improved structures (blue curve) and the ideal structure (red curve) under different h_{top} values. (For interpretation of the references to colour in this figure legend, the reader is referred to the web version of this article.)

conductive and convective thermal transfer processes and given by

$$P_{non-rad}(T_{top}, T_{amb}) = h_{top}(T_{top} - T_{amb}), \tag{8}$$

$$P_{non-rad}(T_{bottom}, T_{amb}) = h_{bottom}(T_{bottom} - T_{amb}), \tag{9}$$

where h_{top} and h_{bottom} are the heat transfer coefficients of the non-radiative process at the top and back surfaces ($W \cdot m^{-2} \cdot K^{-1}$), respectively. For h_{top} and h_{bottom} , two correlations are frequently used for solar energy collectors in previous studies; these two correlations can be expressed as (Tofighi, 2013; Waqas and Ji, 2017) $h_{top} = 5.8 + 3.7u_a$ and $h_{bottom} = 2.8 + 3.0u_a$, where u_a is the velocity of wind ($m \cdot s^{-1}$).

4. Results and discussions

4.1. Experimental results and discussions

4.1.1. Experimental error analysis

Generally, the theory of error propagation is used to calculate the relative error (RE) of the dependent variable y , which can be expressed as follows:

$$y = f(x_1, x_2, x_3, \dots, x_n), \tag{10}$$

$$RE = \frac{dy}{y} = \sum_{i=1}^n \left(\left| \frac{\partial f}{\partial x_i} \right| \frac{dx_i}{y} \right), \tag{11}$$

where x_i ($i = 1, \dots, n$) are related variables of the dependent variable y .

The temperature of the PV module is the final objective. Thus, on

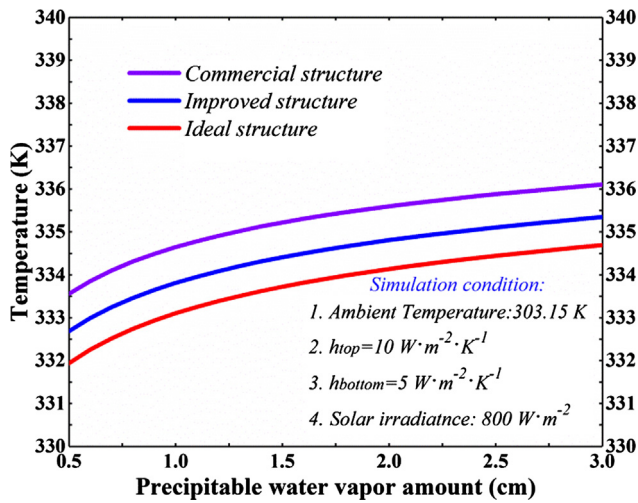


Fig. 9. Temperature of solar cells in the commercial structure (violet curve), improved structure (blue curve), and ideal structure (red curve) under different precipitable water vapor amounts (different sky conditions). h_{top} was set to $10 \text{ W}\cdot\text{m}^{-2}\cdot\text{K}^{-1}$, and h_{bottom} was set to $5 \text{ W}\cdot\text{m}^{-2}\cdot\text{K}^{-1}$ (Li et al., 2017). Ambient temperature and solar radiation were set to 303.15 K and $800 \text{ W}\cdot\text{m}^{-2}$, respectively. (For interpretation of the references to colour in this figure legend, the reader is referred to the web version of this article.)

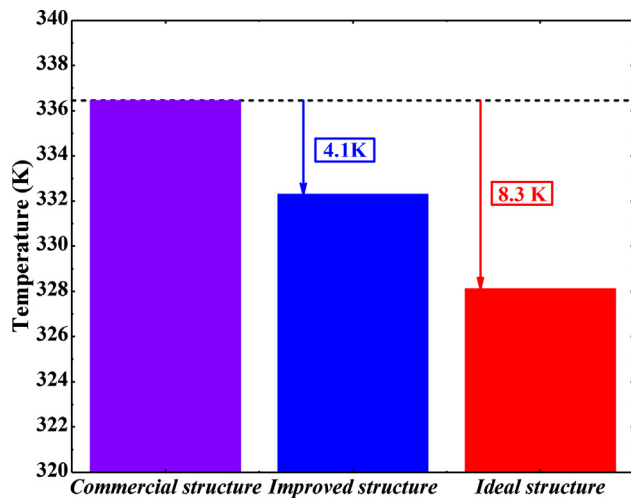


Fig. 10. Temperature of solar cells in the commercial structure (violet), improved structure (blue), and ideal structure (red) in an extraterrestrial environment. The ambient temperature was 3 K , and the solar radiation was $1368 \text{ W}\cdot\text{m}^{-2}$. (For interpretation of the references to colour in this figure legend, the reader is referred to the web version of this article.)

the basis of the uncertainty of the measurement devices presented in Table 1, the maximum RE of the cell’s temperature for commercial and modified structures was determined to be 1.68% and 1.69%, respectively.

4.1.2. Experimental results

The experiment commenced at 10:00 and concluded at 14:00 (March 27, 2018), and the measured data are presented in Fig. 5. The temperature of solar cell in the modified structure was approximately consistent with that in the commercial structure. For example, the average temperature of the solar cell in the modified structure between 11:00 to 13:00 when the solar radiation is relatively strong was $41.4 \text{ }^\circ\text{C}$, which is only $1.0 \text{ }^\circ\text{C}$ lower than that in the commercial structure. When only the influence of such a solar cell temperature reduction was considered, the relative photovoltaic efficiency increased by approximately 0.45%, indicating that the positive effect of the temperature reduction

on photovoltaic conversion improvement was limited. From this point of view, the benefits and prospects of enhanced radiative cooling for cooling solar cells based on commercial PV modules are limited.

4.2. Simulation results and discussions

4.2.1. Validation

A simulation program was written based on the thermal analysis. To validate the mathematical model, root-mean-square deviation (RMSD) was adopted to compare the simulated results with the experimental data. RMSD is a frequently used measure of the deviation between simulated and measured values, and it can be calculated as follows (Bahaidarah et al., 2013):

$$RMSD = \sqrt{\frac{\sum_{i=1}^n [(V_{sim,i} - V_{exp,i}) / V_{exp,i}]^2}{n}}, \quad (12)$$

where V_{sim} is the simulated value, V_{exp} is the measured value, and n denotes the number of data points.

The measured value is the temperature of the bottom surface of the PV module. Thus, the corresponding RMSD was estimated. As shown in Table 2, we selected 13 data points of the bottom surface’s temperature in the modified structure from the experimental data, with 10 min between data points. The corresponding simulated temperature of the bottom surface is also presented in Table 2. The weather data used in the validation process were measured by a meteorological station. Under this condition, the RMSD of the temperature of the bottom surface can be calculated as

$$RMSD(T_{bottom}) = \sqrt{\frac{\sum_{i=1}^{13} [(T_{sim_bottom,i} - T_{test_bottom,i}) / T_{test_bottom,i}]^2}{13}}. \quad (13)$$

The expression reveals that the RMSD of the temperature of the bottom surface was 4.14%, indicating that the simulated results are close to the experimental results, and the thermal analysis model is acceptable for further simulation study.

Two pieces of information should be further clarified. First, the thermal analysis model described in Section 3 is a universal model that has been validated and applied in previous investigations (Li et al., 2017; Zhu et al., 2015, 2014). Second, the effects of conductive and convective heat transfer processes between the PV model and ambient air are crucial because the PV model is exposed to ambient air directly. During the validation, the heat transfer coefficients of conductive and convective heat transfer processes were roughly estimated by two empirical correlations involving wind speed. The measured wind speed was obtained from a meteorological station and may differ from the local wind speed of the PV module. These two rough estimations primarily caused the temperature deviation between the experiment and simulation.

4.2.2. Simulation study

The effects of enhanced radiative cooling on solar cells under different conditions (e.g., solar radiation and sky conditions) were theoretically analyzed. Two spectral optimizations of the commercial structure were selected for the simulation. The spectral emissivity values of the selected optimization were 0.95 (improved structure) and 1.0 (ideal structure); these values were higher than that of the commercial structure. The detailed spectral profiles are plotted in Fig. 6. To ensure the objectivity of the simulative results, we assumed that the solar absorption of the solar cells in the improved and ideal structures is equal to that of the commercial structure.

The temperature of the solar cells in the three structures under different solar radiation types was initially evaluated. h_{top} and h_{bottom} in Eqs. (8) and (9) were set to 10 and $5 \text{ W}\cdot\text{m}^{-2}\cdot\text{K}^{-1}$, respectively, considering the strong non-radiative cooling process for the PV panel in

practical application (Li et al., 2017). Fig. 7a shows that the solar cell temperatures in the three structures were nearly the same. As shown in Fig. 7b, the solar cell temperature difference between the commercial and ideal structures was merely 1.75 K even at $1000 \text{ W}\cdot\text{m}^{-2}$ of solar radiation. This temperature difference corresponded to a relative efficiency improvement of 0.79%.

To investigate the effects of enhanced radiative cooling on solar cells in different structures under different conditions of non-radiative processes, the thermal simulation was restarted by fixing the solar radiation and h_{bottom} to $800 \text{ W}\cdot\text{m}^{-2}$ and $5 \text{ W}\cdot\text{m}^{-2}\cdot\text{K}^{-1}$, respectively, while changing h_{top} . The results are shown in Fig. 8. The commercial structure had the highest solar cell temperature among the three structures, and its solar cell temperature decreased with increased h_{top} . Fig. 8b reveals that the solar cell temperature in the ideal structure was only 3.55 K lower than that in the commercial structure even when h_{top} was zero. This difference corresponded to a relative efficiency improvement of 1.60%.

The sky condition is crucial to radiative cooling. The spectral emissivity of the atmosphere is a fundamental characteristic of the sky condition and can be derived from a single correlation by using the precipitable water vapor amount as the only input parameter (Das and Iqbal, 1987). Herein, the effects of enhanced radiative cooling on solar cells under different sky conditions were investigated by setting different precipitable water vapor amounts. As shown in Fig. 9, the solar cell temperature increased with increased precipitable water vapor amount. This relation indicates that the performance of radiative cooling was weakened by poor sky conditions. However, the temperature differences of the solar cells were almost unchanged. For example, the solar cell temperature in the ideal structure was 1.49 K lower than that in the commercial structure on the average.

For solar cells in an extraterrestrial environment (outer space), a preliminary investigation was conducted as follows. During simulation, solar irradiance was assumed to be fixed at $1368 \text{ W}\cdot\text{m}^{-2}$, and thermal radiation can be radiated outward by the top and bottom surfaces of the solar cell. Fig. 10 indicates that the temperature difference of the solar cells between the commercial and ideal structures was 8.3 K, which corresponded to a relative efficiency advantage of 3.74%.

The simulation studies presented in this section provide two pieces of information. First, enhancing the performance of radiative cooling based on commercial PV modules only slightly affects solar cell cooling for commercial PV modules on terrene. This result indicates that the benefits and prospects of enhanced radiative cooling for cooling solar cells based on commercial PV modules on terrene are limited. Second, the performance of enhanced radiative cooling for solar cells is better in an extraterrestrial environment than on terrene. This finding indicates that radiative cooling can be applied as an alternative method for the thermal management of solar cells in an extraterrestrial environment.

5. Conclusions

The effects of enhanced radiative cooling on solar cells based on commercial PV modules were investigated for practical application. A sample PV module (commercial structure) was fabricated, and its spectral property was optimized by a PDMS film (modified structure). A comparative experiment was conducted, and the results showed that the solar cell temperatures in the commercial and modified structures were nearly the same. Moreover, the effects of enhanced radiative cooling on the PV module under different conditions were analyzed theoretically by a universal mathematical model. The performance of enhanced radiative cooling in cooling solar cells in an extraterrestrial environment was also preliminarily discussed. The detailed results are as follows:

- (1) Enhancing the performance of radiative cooling based on a PV module did not change the cooling effect on solar cells on terrene. Even for the ideal structure in a typical condition, the temperature

reduction was merely 1.75 K, which corresponded to a relative efficiency improvement of 0.79%. This result indicates that the application potential of enhanced radiative cooling is small.

- (2) The effects of enhanced radiative cooling on solar cells can be increased in an extraterrestrial environment. Thus, radiative cooling can be developed as an alternative method for the thermal management of solar cells in an extraterrestrial environment.

Acknowledgments

This work is supported by the National Natural Science Foundation of China (51476159, 51776193, and 51761145109), International Technology Cooperation Program of the Anhui Province of China (BJ2090130038), Fundamental Research Funds for Central Universities, and National Postdoctoral Program for Innovative Talents (BX201700223).

References

- Bagiorgas, H.S., Mihalakakou, G., 2008. Experimental and theoretical investigation of a nocturnal radiator for space cooling. *Renew. Energy* 33, 1220–1227.
- Bahaidarah, H., Subhan, A., Gandhidasan, P., Rehman, S., 2013. Performance evaluation of a PV (photovoltaic) module by back surface water cooling for hot climatic conditions. *Energy* 59, 445–453.
- Bergman, T.L., Lavine, A.S., Incropera, F.P., DeWitt, D.P., 2011. *Fundamentals of Heat and Mass Transfer*, Seventh ed. John Wiley & Sons.
- Chen, Z., Zhu, L., Raman, A., Fan, S., 2016. Radiative cooling to deep sub-freezing temperatures through a 24-h day-night cycle. *Nat. Commun.* 7, 13729.
- Cui, Y., Wang, Y., Huang, Q., Wei, S., 2016. Effect of radiation and convection heat transfer on cooling performance of radiative panel. *Renew. Energy* 99, 10–17.
- Das, A.K., Iqbal, M., 1987. A simplified technique to compute spectral atmospheric radiation. *Sol. Energy* 39, 143–155.
- Dyreson, A., Miller, F., 2016. Night sky cooling for concentrating solar power plants. *Appl. Energy* 180, 276–286.
- Gentle, A.R., Dybdal, K.L., Smith, G.B., 2013. Polymeric mesh for durable infra-red transparent convection shields: Applications in cool roofs and sky cooling. *Sol. Energy Mater. Sol. Cells* 115, 79–85.
- Hu, M., Pei, G., Wang, Q., Li, J., Wang, Y., Ji, J., 2016. Field test and preliminary analysis of a combined diurnal solar heating and nocturnal radiative cooling system. *Appl. Energy* 179, 899–908.
- Kurkjian, C.R., Prindle, W.R., 2005. Perspectives on the history of glass composition. *J. Am. Ceram. Soc.* 81, 795–813.
- Lee, B., Liu, J.Z., Sun, B., Shen, C.Y., Dai, G.C., 2008. Thermally conductive and electrically insulating EVA composite encapsulant for solar photovoltaic (PV) cell. *Express Polym. Lett.* 2, 357–363.
- Li, W., Shi, Y., Chen, K., Zhu, L., Fan, S., 2017. A comprehensive photonic approach for solar cell cooling. *ACS Photonics* 4, 774–782.
- Lu, X., Xu, P., Wang, H., Yang, T., Hou, J., 2016. Cooling potential and applications prospects of passive radiative cooling in buildings: The current state-of-the-art. *Renew. Sustain. Energy Rev.* 65, 1079–1097.
- Man, Y., Yang, H., Spitzer, J.D., Fang, Z., 2011. Feasibility study on novel hybrid ground coupled heat pump system with nocturnal cooling radiator for cooling load dominated buildings. *Appl. Energy* 88, 4160–4171.
- Marti, A., Araujo, G.L., 1996. Limiting efficiencies for photovoltaic energy conversion in multi-gap systems. *Sol. Energy Mater. Sol. Cells* 43, 203–222.
- Raman, A.P., Anoma, M.A., Zhu, L., Rephaeli, E., Fan, S., 2014. Passive radiative cooling below ambient air temperature under direct sunlight. *Nature* 515, 540–544.
- Rephaeli, E., Raman, A., Fan, S., 2013. Ultrabroadband photonic structures to achieve high-performance daytime radiative cooling. *Nano Lett.* 13, 1457–1461.
- Safi, T.S., Munday, J.N., 2015. Improving photovoltaic performance through radiative cooling in both terrestrial and extraterrestrial environments. *Opt. Exp.* 23, A1120–A1128.
- Shockley, W., Queisser, H.J., 1961. Detailed balance limit of efficiency of p-n junction solar cells. *J. Appl. Phys.* 32, 510–519.
- Skoplaki, E., Palyvos, J.A., 2009. On the temperature dependence of photovoltaic module electrical performance: a review of efficiency/power correlations. *Sol. Energy* 83, 614–624.
- Tofighi, A., 2013. Performance evaluation of PV module by dynamic thermal model. *J. Power Technol.* 93, 111–121.
- Waqas, A., Ji, J., 2017. Thermal management of conventional PV panel using PCM with movable shutters – A numerical study. *Sol. Energy* 158, 797–807.
- Zeyghami, M., Goswami, D.Y., Stefanakos, E., 2018. A review of clear sky radiative cooling developments and applications in renewable power systems and passive building cooling. *Sol. Energy Mater. Sol. Cells* 178, 115–128.
- Zhai, Y., Ma, Y., David, S.N., Zhao, D., Lou, R., Tan, G., Yang, R., Yin, X., 2017. Scalable-manufactured randomized glass-polymer hybrid metamaterial for daytime radiative cooling (80–). *Science* 355, 1062–1066.
- Zhou, Z., Sun, X., Bermel, P., 2016. Radiative cooling for thermophotovoltaic systems. *Infrared Remote Sensing and Instrumentation*.
- Zhu, L., Raman, A., Wang, K.X., Anoma, M.A., Fan, S., 2014. Radiative cooling of solar cells. *Optica* 1, 32–38.
- Zhu, L., Raman, A.P., Fan, S., 2015. Radiative cooling of solar absorbers using a visibly transparent photonic crystal thermal blackbody. *Proc. Natl. Acad. Sci.* 112, 12282–12287.